



Amperometric determination of NADH with Co₃O₄ nanosheet modified electrode

Chi-Hao Chen, Ying-Cih Chen, Meng-Shan Lin *

Department of Chemistry, Tamkang University, Tamsui 25137, Taiwan

ARTICLE INFO

Article history:

Received 17 July 2012

Received in revised form

20 October 2012

Accepted 22 October 2012

Available online 10 November 2012

Keywords:

NADH

Metal oxide

Cobalt oxide

Amperometry

ABSTRACT

In this work, we have developed a simple and reliable cobalt oxide (Co₃O₄) based amperometric sensor for the determination of NADH. A sheet shape Co₃O₄ nanooxide was synthesized by the CTAB assisted hydrothermal technique and was characterized by SEM and XPS. Owing to the redox property of Co₃O₄, the operating potential of NADH can be significantly reduced from 0.7 down to 0.1 V. Compared to a commercial Co₃O₄ nanoparticle modified electrode, this nanosheet form cobalt oxide possesses a rapid background subsiding characteristic and a low residual current. This scheme was conducted on a flow injection system with a constant operating potential of 0.1 V (vs. Ag/AgCl, 3 M) in a 0.2 M phosphate buffer at pH 6.0. A suitable linear range from 10 to 100 μM ($R=0.999$) with a detection limit of 4.25 μM ($S/N=3$) was obtained. The RSD for 20 successive measurements of 75 μM NADH is only 1.4%, which indicates a high stability and no contamination during NADH oxidation. This scheme did not suffer from conventional antioxidants, including dopamine, uric acid, epinephrine, serotonin, histamine, and 4-acetaminophen, except ascorbic acid. Thus, an ascorbate oxidase was introduced to remove the ascorbic acid before the sample was injected into the flow injection analysis system. After this simple pretreatment, the influence of ascorbic acid was eliminated, successfully.

© 2012 Elsevier B.V. All rights reserved.

1. Introduction

NAD⁺ and its reduced form, NADH, are important cofactors in the electron transport chain. More than 300 biological enzymatic reactions require NAD⁺ as a cofactor to receive the electron after a particular dehydrogenated reaction. Thus, the merits of a NAD⁺/NADH sensor are critical due to its possible application in the development of dehydrogenase based biosensors as well as their applications in food processing, environmental analysis, and clinical diagnosis. Several optical approaches have been reported in the determination of the NADH; generally, measuring the absorption of NADH at 340 nm is widely used in identification of enzymatic activity (McComb et al., 1976). Subsequently, because the excited NADH is a suitable fluorophore which has a strong emission at 450 nm, a further fluorescence method provides a high sensitivity in the NADH determination (Podrazky and Kuncova, 2005). In addition, NADH is a suitable co-reactant for the Ru (bpy)₃²⁺ that enhances the electrochemical luminescence (ECL); several ECL based approaches have been reported to provide a highly sensitive scheme to monitor the NADH at nanomolar level (Martin and Nieman, 1997; Deng et al., 2009).

Actually, NADH is a famous reductant in biological systems with a formal reduction potential of -0.32 V vs. NHE (Nelson and Cox, 2005), and electrochemical determination of NADH is a critical issue. However, direct oxidation of NADH required a relatively high overpotential at bare electrodes (Eisenberg and Cundy, 1991; Wang et al., 2001) and usually causes a passive layer to pollute the surface of the electrode (Radoi et al., 2008). Keita and Sampath indicated that this problem is attributed to its electrochemical product which would adsorb onto the surface after self dimerization (Keita et al., 1996; Sampath and Lev, 1998). Besides, the crucial overpotential limits its application in real biological samples from most co-existed antioxidants. In order to overcome this problem, several carbon based materials such as carbon nanotube (Pumera et al., 2006), carbon fiber (Zhao et al., 2010), pyrolytic glassy carbon (Banks and Compton, 2005), and graphene (Keeley et al., 2011) have been proposed to show its facilitation in electrochemical oxidation of NADH; however, the catalytic potential of these carbon based sensors can be shifted down to only around 0.4 V, and analytical result would be still affected by most biological antioxidants.

To solve these dilemmas, several redox mediators were employed to provide another pathway in the catalytic oxidation of NADH. The most popular organic modifiers can be roughly divided into fluorenone (Mano and Kuhn, 1999), phenothiazine (Boguslavsky et al., 1995), phenoxazine (Kubota et al., 1996), and quinone (Jaegfeldt et al., 1981) based modifiers according to their

* Corresponding author. Tel.: +886 2 26215656x2542; fax: +886 2 26299996.
E-mail address: mshlin@mail.tku.edu.tw (M.-S. Lin).

basic chemical structure. These mediators could be easily adsorbed on the electrode surface through physical or electrostatic interaction. Generally, the operating potential used in a physically adsorbed modified sensor could be down to less than 0 V; however, these sensors can be operated only in a static condition due to the weak interaction between the surface and the modifier. Electrochemical polymerization provides a more secure scheme to immobilize these mediators on the electrode surface which can be easily held on high convective situation such as a flow injection system and a rotating analysis; however, the catalytic potential of the most polymerized electrode shows a positive shift compared to that of a free molecule. For example, the catalytic potential of a methylene blue modified electrode is -0.036 V (Borgo et al., 2002), but a polymeric electrode required 0.15 V to achieve this approach (Dilgina et al., 2011). Toluidine blue/CNT electrode possesses a catalytic potential at -0.2 V (Lawrence and Wang, 2006), but shifted toward 0.2 V after polymerization (Hasebe et al., 2011).

The application of nanometal or metal oxide particles has emerged as an attractive investigation in recent years. Since the chemical and physical properties of nanomaterials are different from bulk ones, a number of research fields are successful in obtaining a remarkable progress after working with nano materials. Several fabricated techniques, including sol-gel (Laberty-Robert et al., 2006), co-precipitation (Quin and Shi, 1998), and hydrothermal method (Hagrman et al., 2001), have been widely demonstrated. Among these schemes, the hydrothermal method is considered as an attractive method to fabricate nanometal oxides. By controlling the temperature and pressure, a metastable material has been produced (Zhang et al., 2003). In addition, the morphology of the nanostructure is varied according to the conformation of the micelle (Wang et al., 2011). Generally, ethylene diamine tetraacetic acid, sodium dodecyl sulfate, polyethyleneglycol and hexadecyltrimethylammonium bromide (CTAB) have been frequently used as templates in hydrothermal techniques.

Recently, metal oxide based modified electrodes have intensively investigated in the electrochemical determination of several clinical markers due to their interesting catalytic properties (Chen and Lin, 2012; Shih et al., 2009; Zen et al., 2002). However, their application in NADH is still rare. To the best of our knowledge, only $\text{Fe}_3\text{O}_4/\text{CNT}$ modified electrode has been reported to show its catalytic oxidation of NADH at 0 V (Teymourian and Salimi, 2012); however, that report used an acid pre-treated carbon nanotube as its basic matrix, and this matrix has been proven to possess a similar catalytic behavior to that of the NADH at 0 V (Wooten and Gorski, 2010); hence, the role of Fe_3O_4 in the catalytic determination of NADH still needs to be investigated. In this work, the feasibility of catalytic oxidation of NADH by using the redox property of Co_3O_4 is reported. In order to overcome the drawbacks of highly residual current and sluggish response of Co_3O_4 modified electrode, a nanosheet Co_3O_4 synthesized by the CTAB assisted hydrothermal technique was used in this study, which provides a simple and sensitive method with limited interference. The possible mechanism and the analytical performance are also described in this report.

2. Material and methods

2.1. Apparatus

A CHI 832B electrochemical workstation (CH Instruments Austin, TX, USA) was used in the whole electrochemical studies. The flow rate of the FIA system was controlled with a syringe pump (74900 series, Cole-Parmer Instrument Company, Illinois,

USA). A steel reactor containing a Teflon vessel was used to synthesize the Co_3O_4 nanosheet. The surface morphology of nanosheet was taken by FE-SEM (LEO1530, Germany) and X-ray Photoelectron Spectroscopy (XPS) was performed by ESCALAB 250 (Thermal VG science, UK). A Ag/AgCl (3 M NaCl) electrode was used as the reference electrode in this scheme.

2.2. Reagents

Cobalt (II) nitrate hexahydrate, and NADH (98%) were purchased from Acros Organics. Urea (99.5%) was obtained from Riedel-dehaën (Seelze, Germany). Serotonin hydrochloride (99%) was purchased from Alfa-Aesar. Hexadecyltrimethylammonium bromide (CTAB, 99%), L (+)-ascorbic acid (99.7%), uric acid, dopamine, histamine (99%), (\pm)-epinephrine (95%), 4-acetaminophenol, Co_3O_4 nano particle, and CoO were obtained from Sigma-Aldrich (St. Louis, USA). All other chemicals and solvents were of analytical grade and were used as received without further purification. A conductive carbon ink (C10903D14) obtained from Gwent Electronic Materials Ltd. (Pontypool, UK) was used for immobilization of CoO, and Co_3O_4 on the electrode. Ascorbate oxidase (EC 1.10.3.3) was purchased from TOYOBO (Osaka, Japan).

2.3. Fabrication of Co_3O_4 nanosheet

The Co_3O_4 nanosheet was fabricated according to the previous report with certain modification (Liu et al., 2007). Briefly, 6 mmole $\text{Co}(\text{NO}_3)_2$, 45 mmole urea, and 3 g CTAB were dissolved in a Teflon container containing 100 mL water. Subsequently the container was sealed in a stainless steel reactor. A purple-red cobalt complex would be obtained after sequentially heating at 70 °C and 120 °C for 24 h and 12 h, respectively. This complex was dried in an oven at 70 °C overnight and calcined in a tube furnace (F-21100, Thermolyne, USA) at 600 °C for 2 h to remove the organic template and convert their oxidation state into Co_3O_4 .

2.4. Procedure of electrode modification and mechanism study

A homemade rotating disc carbon electrode with a diameter of 5 mm was used in the hydrodynamic voltammetry and potentiometric study. This Co_3O_4 modified electrode was constructed by weighting appropriate Co_3O_4 nanosheet, conducting ink and cyclohexanone. The final weight ratio of this suspension mixture is 7:3:20. Subsequently, 2.5 μL of above mixture was placed on the electrode surface and allowed to dry in an oven at 70 °C for 1 h. When not in use, it was kept in a dry container full of nitrogen at room temperature. A dual rotating ring-disk platinum electrode (BAS, IN, USA) immobilized with 70% CoO powder on the central disk electrode was used to investigate the final product of oxygen reduction. A simple potentiometric study by measuring the potential difference between modified electrodes and the reference electrode (Ag/AgCl, 3 M NaCl) was used to evaluate the oxidation state of cobalt oxide.

3. Results and discussion

3.1. Characterization of Co_3O_4 nanosheet

The morphology of the prepared cobalt oxide was characterized by scanning electron microscopy (SEM). Fig. 1A shows a typical SEM image of the Co_3O_4 nanosheet with magnification of 10,000 folds. This image shows that this microscale particle is constructed from several nano rectangular sheets. Further magnification with 100,000 folds as shown in Fig. 1B indicates that

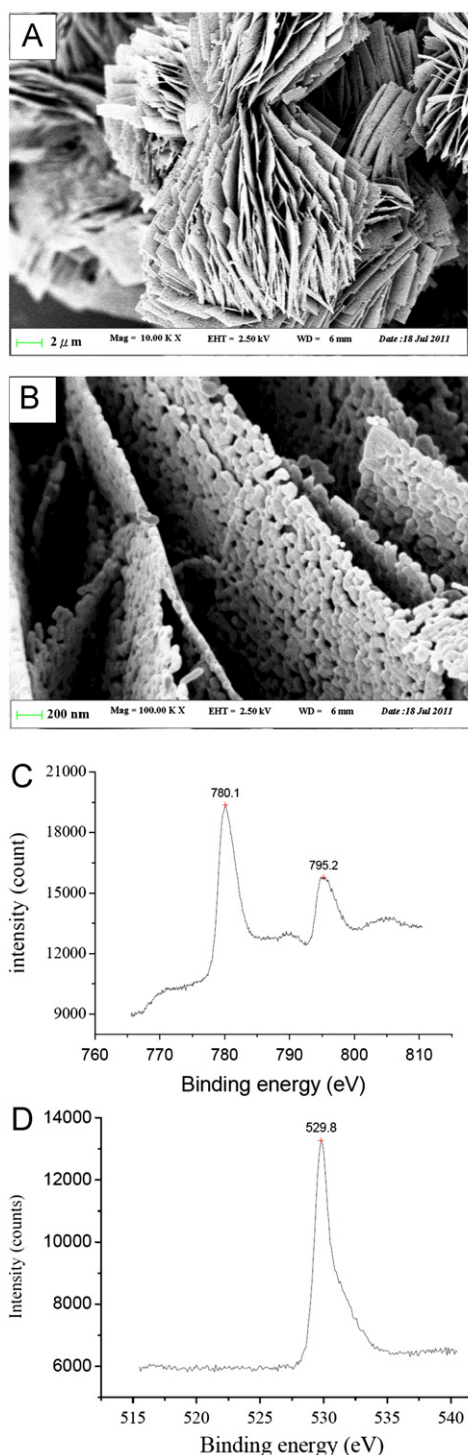


Fig. 1. SEM picture of Co_3O_4 nano sheet with magnification of $10,000\times$ (A), and $100,000\times$ (B). The range of binding energy in XPS spectra corresponds to cobalt 2p (C) and oxygen 1s orbital (D), respectively.

this nanosheet was constructed from orderly cobalt oxide nanoparticles. Although a cobalt (II) ion was used as the precursor in the hydrothermal process, the oxidation state of cobalt oxide can be further regulated by the temperature. Here this cobalt oxide was calcined at 600°C for 2 h to ensure that Co_3O_4 is the major state (Greenwood and Earnshaw, 1984). However, in order to clearly identify the oxidation state, the prepared cobalt oxide was characterized by XPS as shown in Fig. 1C. The peaks with a binding energies of 780.1 and 795.2 eV are assayed corresponding

to $2p_{3/2}$ and $2p_{1/2}$, respectively. A typical energy difference of 15.1 eV and no significant shake-up satellite peaks indicate that the oxidation state of this cobalt oxide is Co_3O_4 (Barreca and Massignan, 2001). The oxidation state was further identified by using a potentiometric test. In an anaerobic phosphate buffer, pH 6, the open circuit potential (OCP) of 70% nanosheet cobalt modified electrode was measured at 0.374 V (vs. Ag/AgCl, 3 M NaCl), which is much higher than a 70% CoO modified one (around 0.04 V). These results indicate that this nanosheet is Co_3O_4 rather than CoO. In addition, Fig. 1D shows a clear spectrum of oxygen 1s without a significant branch peak, which indicates a limited impurity adsorbed on the Co_3O_4 surface (Wang et al., 2010).

3.2. Promotion and catalytic mechanism of Co_3O_4 nanosheet modified electrode

It is known that a huge residual current is the major drawback that limits the analytical usage of a metal oxide based electrochemical sensor. Fig. S1 shows typical amperometric responses obtained from a 50% commercially available Co_3O_4 modified electrode (A) and a nanosheet one (B) when the operated potential stepped from 0 to 0.25 V. We found that the background current of the nanosheet modified one subsides rapidly to 10^{-7} A level within 250 s; however, the commercially available one remains with a high residual current of around 5.0×10^{-7} A. Furthermore, the stable residual current of nanosheet modified electrode can decrease down to 10^{-8} A level; however, the commercial one is still as high as 3.0×10^{-7} A with a sluggish decrement. These results indicate that this nanosheet possesses a smaller capacity current and reaches its steady state, rapidly. In addition, the lower background level also facilitated to acquiring an efficient LOQ and detection limit.

It is well known that electrochemical oxidation of NADH would cause a fouling problem in the electrode. In order to demonstrate the catalytic capability and reproducibility of this Co_3O_4 nanosheet modified electrode, a hydrodynamic voltammetry was conducted on a rotating electrode system to acquire the steady state responses. Fig. 2A shows the typical potential profile of $30\ \mu\text{M}$ NADH on a 70% Co_3O_4 nanosheet modified electrode (a) and its matrix, and conductive ink electrode (b) from 0 to 0.6 V with an interval of 0.05 V. It is noticed that the minimum oxidation potential of the NADH on a bare carbon ink electrode should be beyond 0.4 V; however, the catalytic potential of the Co_3O_4 modified one can be reduced to 0.05 V. This catalytic behavior should be attributed to the alteration of the oxidation state of Co_3O_4 rather than any functional group that existed on the carbon surface. In order to confirm this assumption, a simple potentiometry was conducted again to trace the oxidative state of Co_3O_4 modified electrode as shown in Supplementary in Fig. S2. In an anaerobic phosphate buffer at pH 6.0, the OCP of 70% Co_3O_4 modified electrode is stable at around 0.37 V. However, this OCP decreased to 0.06 V after addition of a 0.5 mM NADH into the buffer. This result indicates that Co_3O_4 can be reduced chemically by NADH. Based on the previous discussions, a possible mechanism is shown in Scheme 1. Briefly, Co_3O_4 was reduced to CoO by NADH; in the meantime, an oxidation potential was applied to convert the CoO back to Co_3O_4 , and this oxidative current was used to reflect the concentration of the NADH.

3.3. Effect of oxygen tension

In the previous section, we have shown that Co_3O_4 would be reduced to CoO after reaction with NADH, and the catalytic current of this scheme is attributed to the oxidation of CoO back to the Co_3O_4 . However, because CoO has been also reported to

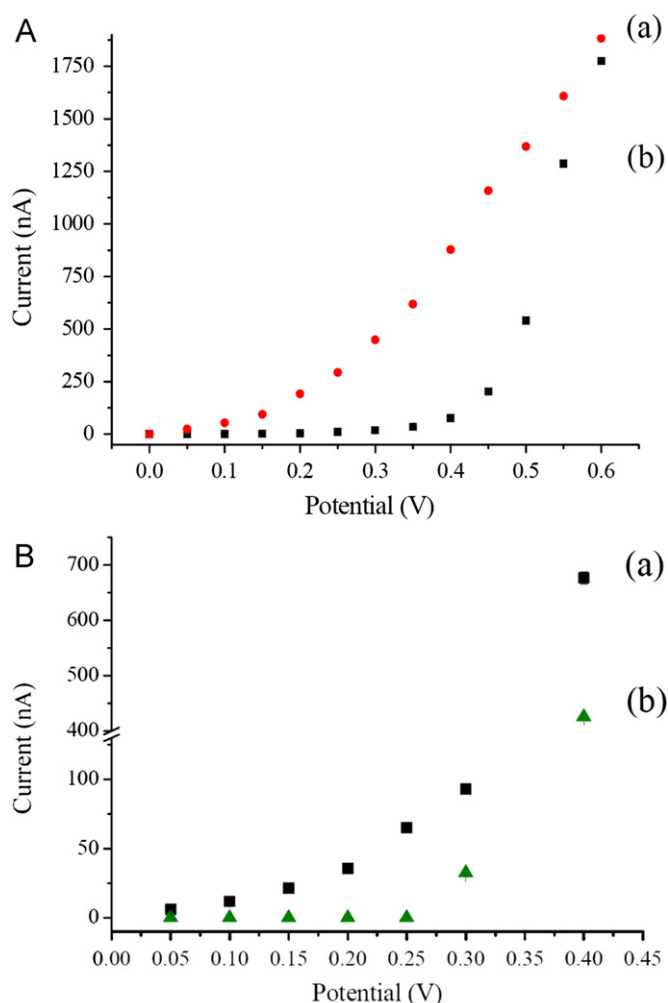
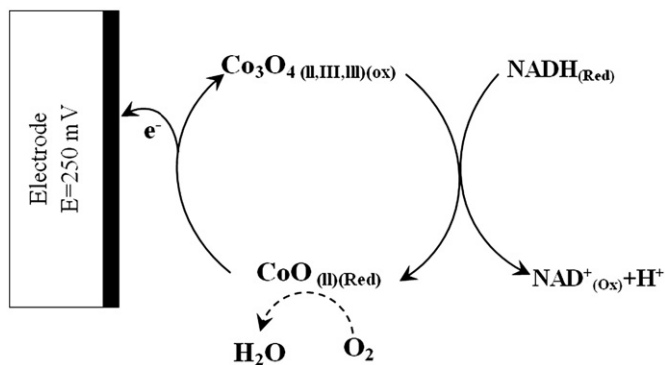


Fig. 2. Dynamic potential studies of NADH from a rotating electrode system at 625 rpm (A) and from flow injection analysis (B). The current intensity in graph A was recorded from the steady state oxidative current of 30 μM NADH on 70% Co_3O_4 (a) and bare carbon ink electrode (b). The current responses in graph B correspond to an injection of 25 μM NADH (a) and uric acid (b), at a flow rate of 0.25 mL/min.



Scheme 1. Proposed NADH measurement mechanism on a Co_3O_4 based electrode.

facilitate the oxygen reduction (Hamdani et al., 2010), the influence of the oxygen to this scheme is discussed in this work. Supplementary in Fig. S3 shows the current response of 25, 50 and 75 μM NADH at a potential of 0.25 V in various oxygen tensions. The sensitivities are 17.2, 10.7, and 7.3 $\text{nA}/\mu\text{M}$ corresponding to anaerobic (A), ambient (B), and saturated (C) oxygen tensions, respectively. Besides, in the mass transfer independent

situation, the limiting current of 25 μM NADH decreased significantly from $319.2 \pm 1.5 \text{ nA}$ to $226 \pm 3.8 \text{ nA}$ in the presence of oxygen (see the supplementary Fig. S4). According to the intensity of the limiting current, the rate constant of this scheme is calculated as $2.34 \pm 0.01 \times 10^{-3} \text{ cm/s}$ in an anaerobic situation and $1.66 \pm 0.03 \times 10^{-3} \text{ cm/s}$ in an ambient solution. These results imply that the reduced CoO would be directly oxidized by the oxygen, and a portion of the electron would be transferred from CoO oxygen.

The final product of oxygen after reaction with the CoO is another interesting issue. In general, hydrogen peroxide and water are two possible products after obtained reduction of oxygen. In order to define this final product, a generation–collection study was conducted by using a platinum rotating ring–disk electrode. Here, the central disk electrode was covered with 70% CoO as a generator to directly react with the oxygen; a constant potential of 0.7 V was applied on the ring electrode to detect the oxidation signal of hydrogen peroxide if it was really produced during oxygen reduction. However, no significant oxidation current could be found after spiking 5 mL ambient buffer solution into the original anaerobic buffer solution (data not shown). This result implies that hydrogen peroxide might not be the major product of this reaction. This inference was also proved by using the potentiometric test. Supplementary in Fig. S5 traced the OCP of 70% CoO modified electrode after addition of oxygen and hydrogen peroxide. In an anaerobic condition, the OCP of CoO modified electrode is stable around 0.06 V, which is much lower than that of the Co_3O_4 modified electrode (around 0.37 V). The OCP increased sluggishly to 0.12 V when oxygen tension recovered to the ambient situation. However, this OCP shows a sharp and rapid increment toward 0.25 V after addition of 0.5 mM hydrogen peroxide. This result implies that both oxygen and hydrogen peroxide can oxidize the CoO oxide, but the reaction rate of hydrogen peroxide might be much faster than that of oxygen. According to the prior discussions, hydrogen peroxide might be produced during this reaction; however, this intermediate would be further oxidized by the CoO layer, immediately. Thus, water might be more possible to be obtained as the final product.

3.4. Optimization of flow injection analysis

In order to develop a prompt and highly sensitive analytical method, this NADH sensor was evaluated in a flow injection system. The operating potential was optimized firstly due to the concern with the sensitivity and selectivity. Since the problem of surface contamination has been widely reported in the previous studies, here, this potential study was limited below 0.4 V to elude the direct oxidation of NADH on the carbon matrix. Fig. 2B shows the catalytic current of 25 μM NADH (a), and the major interference, uric acid (b) in various operating potentials. It is observed that the NADH can be catalytically oxidized at 0.05 V; however, the influence of uric acid can be ignored before 0.25 V. Thus, 0.25 V was chosen as the optimal potential for the subsequent study. The influence of buffer acidity that ranged from pH 5 to 8 was investigated as shown in supplementary Fig. S6. The current response decreases slightly with a slope of 7.1 nA/pH as pH increases. However, uric acid becomes a significant interference when pH is higher than 6.5, moreover, the interference of uric acid is even tripled than that of NADH at pH 8. Thus, pH 6 was chosen as the optimal buffer acidity for the subsequent analysis. Other conditions, including flow rate, sample volume, buffer concentration and composition, were optimized. After considering the current sensitivity and stability, 200 mM phosphate buffer solution, pH 6 with sample injected volume of 50 μL and the flow

rate of 0.25 mL/min were chosen as the optimal conditions (data not shown).

3.5. Analytical performance and interference study

After optimization of the major operating conditions as discussed in the previous section, Fig. 3 shows a typical calibration plot of this proposed scheme at 0.25 V. A linear range starting from 1 μM to 30 μM ($R^2=0.999$) with a sensitivity of 2.76 nA/ μM is obtained. The detection limit estimated from the slope of calibration plot and the standard deviation of 21 successive buffer injections as blank is 0.53 μM ($S/N=3$). Moreover, a transient sensitivity between 30 and 50 μM and a second linearity from 50 to 150 μM with a sensitivity of 1.43 nA/ μM ($R^2=0.999$) are observed; this result implies that the reaction rate might change from a diffusion controlled behavior into a kinetically controlled one. Table 1 summarized the analytical performances of the present scheme and other NADH electrochemical sensors reported previously. The limit of quantification (LOQ) and operating potential of our scheme are better than in several previous reports such as those of pyrolytic graphite electrode (Banks and Compton, 2005), graphene modified glassy electrode (Keeley et al., 2011), $\text{TiO}_2/\text{MCM-41}$ modified glassy carbon electrode

(Dai et al., 2007), and poly(1,2-DAB) nanotube modified glassy carbon electrode (Valentini et al., 2004). Table 2 shows the interference study of several biological antioxidants. The influences of serotonin, histamine, acetaminophen and uric acid are negligible; however, this scheme would be affected by dopamine, epinephrine and ascorbic acid. The previous two interferences can be eliminated by reducing the operating potential to 0.1 V, but the method still fails to deal with the interference caused by ascorbic acid. Here, we use the ascorbate oxidase to oxidize the ascorbic acid, previously. Supplementary Table S2 shows that the influence of ascorbic acid and the discrepancy of oxygen consumption during enzymatic reaction can be totally ignored after reaction with the AAO for 5 min. Subsequently, the analytical performance of the current scheme at a potential of 0.1 V is shown in Table 1. Although the sensitivity decreased from 2.76 to 0.36 nA/ μM , this method can be carried out in an ambient condition and still yields sensors comparable with several successful NADH sensors such as poly(p-ABSA)/FAD modified electrode (Kumar and Chen, 2007a), medola blue/ZnO electrode (Kumar and Chen, 2007b) as well as the Nile Blue/ZrP/carbon paste electrode (Pessoa et al., 1997). Finally, the reproducibility is evaluated by calculating the variation of 20 successive injections of 75 μM NADH. We found the RSD of the signal is only 1.4%, which indicates a high stability and no contamination effect of the current scheme.

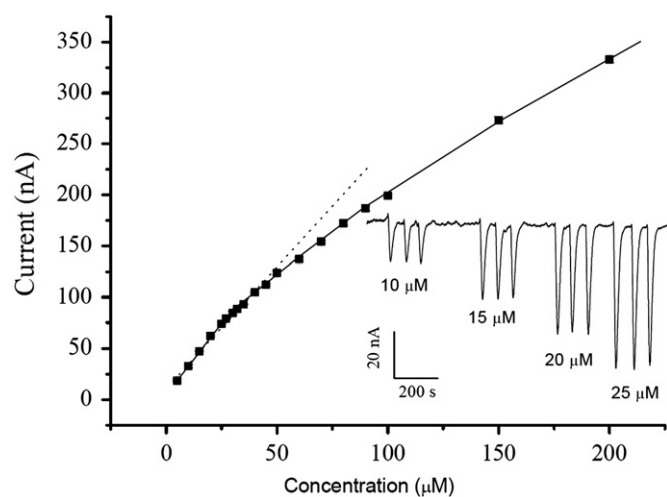


Fig. 3. Typical calibration plot of NADH at constant potential of 0.25 V. The inset diagram is the actual responses of sequential injection of 10, 15, 20, and 25 μM NADH.

Table 1

Comparison of the analytical performance of the NADH sensor based on the amperometric schemes. The abbreviations of GC, ABSA, MCM-41, and 1,2 DAB are glassy carbon, aminobenzene sulfonic acid, mobile crystalline material-41, and 1, 2 diaminobenzene, respectively. All the potentials refer to a Ag/AgCl electrode.

Amperometric NADH sensing method: critical technique	Potential (V)	Linearity	Detection limit (μM)	Reference
Graphene/GC	0.4	Up to 360 μM	1.9 μM	Keeley et al. (2011)
Nano-Au/ SiO_2/GC	0.40 ^b	1–100 μM	– ^a	Liu et al. (2010)
Benzoquinone/graphite	0.15	1–10 mM	– ^a	Murthy and Sharma (1998)
Pyrolytic graphite/GC	0.45	2.25–36 μM	1	Banks and Compton (2005)
poly(p-ABSA)/FAD/GC	0.2	10–300 μM	1	Kumar and Chen (2007a)
Meldola blue/ZnO	0	50–300 μM	10	Kumar and Chen (2007b)
Nile blue/ZrP/carbon paste	0.095 ^b	0.1–2 mM	5	Pessoa et al. (1997)
$\text{TiO}_2/\text{MCM-41}/\text{GC}$	0.32 ^b	0.01–1.2 mM	8	Dai et al. (2007)
Poly(1,2-DAB) nanotube/GC	0.45	0.05–1 mM	– ^a	Valentini et al. (2004)
Co_3O_4 nanoparticle/carbon ink	0.25	1–40 μM	0.61	This work
Co_3O_4 nanoparticle/carbon ink	0.1	15–125 μM	5.74	This work
Co_3O_4 nano sheet/carbon ink	0.25	1–30 μM	0.53	This work
Co_3O_4 nanosheet/carbon ink	0.1	10–100 μM	4.23	This work

^a No data.

^b Adjust the discrepancy of reference potential from a SCE to a Ag/AgCl electrode.

Table 2

The interference studies of Co_3O_4 modified electrode at potential of 0.25 V and 0.1 V.

Test compound	Concentration (μM)	Interference ratio (%) ^a		
		0.25 V	0.1 V	0.1 V, AAO ^b
Dopamine	10	264.0	N.D.	N.D.
(\pm)-Epinephrine	10	282.4	N.D.	N.D.
Serotonin	10	3.8	N.D.	N.D.
Histamine	10	N.D. ^c	N.D.	N.D.
4-Acetaminophenol	100	N.D.	N.D.	N.D.
Uric acid	25	N.D.	N.D.	N.D.
L(+)-Ascorbic acid	40	460.2	652.7	N.D.

^a Interference = $(I_1/I_0) \times 100\%$, where I_1 is the response of the test compound and I_0 is the current response of 25 μM NADH.

^b The sample was pretreated by ascorbic acid oxidase (2 units/mL) for 5 min.

^c Not detected.

4. Conclusion

We have demonstrated the feasibility of oxidation determination of NADH catalytically by using a Co_3O_4 modified electrode. This nanosheet based Co_3O_4 shows a lower background level and prompt response during alteration of the applying potential. A simple OCP measurement gives straight-forward evidence to investigate the whole catalytic mechanism and the chemical product of oxygen. This method can provide a more stable, convenient, and rapid method for NADH determination. Moreover, the conducting carbon ink provides a convenient scheme to trap this Co_3O_4 nanosheet by using a simple blending method; further applications, including its use in several dehydrogenase based biosensors and disposable strips, are investigated intensively in our laboratory.

Acknowledgment

We are grateful for the financial support from the National Science Council in Taiwan (Grant no. NSC 100-2113-M-032-001-MY3).

Appendix A. Supporting information

Supplementary data associated with this article can be found in the online version at <http://dx.doi.org/10.1016/j.bios.2012.10.086>.

References

- Banks, C.E., Compton, R.G., 2005. *Analyst* 130, 1232–1239.
- Barreca, D., Massignan, C., 2001. *Chemistry of Materials* 13, 588–593.
- Boguslavsky, L.I., Geng, L., Kovalev, I.P., Sahni, S.K., Xu, Z., Skotheim, T.A., 1995. *Biosensors and Bioelectronics* 10, 693–704.
- Borgo, C.A., Lazzarin, A.M., Gushikem, Y., 2002. *Sens. Sensors and Actuators B: Chemical* 87, 498–505.
- Chen, C.H., Lin, M.S., 2012. *Biosensors and Bioelectronics* 31, 90–94.
- Dai, Z., Lu, G., Bao, J., Hyang, X., Ju, H., 2007. *Electroanalysis* 19, 604–607.
- Deng, L., Zhang, L., Shang, L., Guo, S., Wen, D., Wang, F., Dong, S., 2009. *Biosensors and Bioelectronics* 24, 2273–2276.
- Dilgina, Y., Dilgin, D.G., Dursun, Z., Gökçel, H.İ., Gligor, D., Bayrak, B., Ertek, B., 2011. *Electrochimica Acta* 56, 1138–1143.
- Eisenberg, E.J., Cundy, K.C., 1991. *Analytical Chemistry* 63 (8), 845–847.
- Greenwood, N.N., Earnshaw, A., 1984. *Chemistry of the Elements*, 1st ed. Butterworth-Heinemann, Oxford 1296–1297.
- Hagman, P.J., Finn, R.C., Zubieta, J., 2001. *Solid State Sciences* 3, 745–774.
- Hamdani, M., Singh, R.N., Chartier, P., 2010. *International Journal of Electrochemical Science* 5, 556–577.
- Hasebe, Y., Wang, Y., Fukuoka, K., 2011. *Journal of Environmental Sciences* 23, 1050–1056.
- Jaegfeldt, H., Torstensson, A.B.C., Gorton, L.G.O., Johansson, G., 1981. *Analytical Chemistry* 53, 1979–1982.
- Keeley, G.P., Neill, A., Holzinger, M., Cosnier, S., Coleman, J.N., Duesberg, G.S., 2011. *Physical Chemistry Chemical Physics* 13, 7747–7750.
- Keita, B., Essaadi, K., Nadjo, L., Contant, R., Justum, Y., 1996. *Journal of Electroanalytical Chemistry* 404, 271–279.
- Kubota, L.T., Gouvea, F., Andrade, A.N., Milagres, B.G., Neto, G.D.O., 1996. *Electrochimica Acta* 41, 1465–1469.
- Kumar, S.A., Chen, S.M., 2007a. *Sensors and Actuators B: Chemical* 123, 964–977.
- Kumar, S.A., Chen, S.M., 2007b. *Analytica Chimica Acta* 592, 36–44.
- Laberty-Robert, C., Long, J.W., Lucas, E.M., Pettigrew, K.A., Stroud, R.M., Doescher, M.S., Rolison, D.R., 2006. *Chemistry of Materials* 18, 50–58.
- Lawrence, N.S., Wang, J., 2006. *Electrochemistry Communications* 8, 71–76.
- Liu, Q., Zhang, W., Cui, Z., Zhang, B., Wan, L., Song, W., 2007. *Microporous and Mesoporous Materials* 100, 233–240.
- Liu, X., Li, B., Wang, X., Li, C., 2010. *Microchimica Acta* 171, 399–405.
- Mano, N., Kuhn, A., 1999. *Journal of Electroanalytical Chemistry* 477, 79–88.
- Martin, A.F., Nieman, T.A., 1997. *Biosensors and Bioelectronics* 12, 479–489.
- McComb, R.B., Bond, L.W., Burnett, R.W., Keech Jr, R.C., Bowers, G.N., 1976. *Clinical Chemistry* 22, 141–150.
- Murthy, A.S.N., Sharma, J., 1998. *Talanta* 45, 951–956.
- Nelson, D.L., Cox, M.M., 2005. fourth ed. *Principles of Biochemistry*, 695. W.H. Freeman and Company, New York.
- Pessoa, C.A., Gushikem, Y., Kubota, L.T., Gorton, L., 1997. *Journal of Electroanalytical Chemistry* 431, 23–27.
- Podrazky, O., Kuncova, G., 2005. *Sensors and Actuators B: Chemical* 107, 126–134.
- Pumera, M., Merkoc, A., Alegret, S., 2006. *Sensors and Actuators B: Chemical* 113, 617–622.
- Quin, Z., Shi, J.L., 1998. *Nanostructured Materials* 10, 235–244.
- Radoi, A., Compagnone, D., Valcarcel, M.A., Placidi, P., Materazzi, S., Moscone, D., Palleschi, G., 2008. *Electrochimica Acta* 53, 2161–2169.
- Sampath, S., Lev, O., 1998. *Journal of Electroanalytical Chemistry* 446, 57–65.
- Shih, W., Yang, M., Lin, M.S., 2009. *Biosensors and Bioelectronics* 24, 1679–1684.
- Teymourian, H., Salimi, A., 2012. *Biosensors and Bioelectronics* 33, 60–68.
- Valentini, F., Salis, A., Curulli, A., Palleschi, G., 2004. *Analytical Chemistry* 76, 3244–3248.
- Wang, C., Wang, D., Wang, Q., Wang, L., 2010. *Electrochimica Acta* 55, 6420–6425.
- Wang, J., Chatrathi, M.P., Tian, B., 2001. *Analytical Chemistry* 73, 1296–1300.
- Wang, Y., Sun, J., Fan, X., Yu, X., 2011. *Ceramics International* 37, 3431–3436.
- Wooten, M., Gorski, W., 2010. *Analytical Chemistry* 82, 1299–1304.
- Zen, J.M., Lai, Y.Y., Yang, H.H., Kumar, A.S., 2002. *Sensors and Actuators B: Chemical* 84, 237–244.
- Zhao, X., Lu, X., Tze, W.T.Y., Wang, P., 2010. *Biosensors and Bioelectronics* 25, 2343–2350.
- Zhang, Y., Wang, H., Wang, B., Xu, H., Yan, H., Yoshimura, M., 2003. *Optical Materials* 23, 433–437.